5-Axis AMB Suspension Design for 300 HP Industrial Compressor

Paul Allaire[a], Brad Nichols[a], Tim Dimond[a], Jianming Cao[a], Xianhao Ma[b], Raojing Shang[b], Chunyan Wang[b],Huajun Wang[b]

[a] Rotor Bearing Solutions International, LLC, 805 Emerson Drive, Charlottesville, VA, 22901, USA, paul.allaire@rotorsolution.com
[b] Suzhou Palboom Electric Co., Ltd., 1/F, Building B, Fenghuang Avenue 7, 39501 Suzhou City, China

***Abstract*— This paper provides the design methodology, bearing geometries, and specifications for both the radial and axial AMBs as designed for an industrial 300 HP motor-blower unit. For each bearing design, the design principles and corresponding 1D circuit models are methodically presented and discussed. Next, the optimized bearing geometries and bearing properties are presented. The algorithms used by the design software, based on the 1D circuit model bearing analyses, refine the design process and verify the results using 2D finite element analysis (FEA). Based on calculated loads for the radial bearing and estimated loads for the thrust bearing, the radial AMB is designed for a load capacity of 2,000 N while the thrust bearing is designed for a load capacity of 3,000 N. The maximum rotational speed of the 200 KW unit is considered to be 21,000 rpm.**

I. INTRODUCTION

This paper presents the design schematic of a full magnetic bearing suspension system for a high speed industrial motor compressor operating up to 21,000 rpm. It is a single stage, overhung impeller with a 200 KW motor, in a horizontal configuration, supported by two radial magnetic bearings, as shown in Fig. 1. It also has a thrust bearing for axial loading, due to forces acting on the compressor impeller. The thrust bearing is placed outside of the radial impeller end radial bearing for more easy assembly and to keep the axial clearance of the impeller to a significant distance when heating of the rotor occurs. Two backup (auxiliary bearings) have been placed in the unit for rotor drop protection in the event of power loss.

The rotor schematic is given in Fig. 2. It includes the steel shaft, motor rotor lamination stack, impeller, radial AMB lamination stacks, thrust disk and backup bearing landing sleeves. The rotor operating speed is 20,000rpm, the rotor total weight is 97.2 kg, and the overall length is 952 mm. The magnetic bearing system is 5 axes, 2 radial and 1 thrust. There are 2 touchdown bearings, angular contact double row ceramic ball bearing without a cage, as illustrated in Fig. 1. The shaft diameter under the AMB lamination stacks is 110 mm.

Magnetic bearing design has a long history of development over the past 40 years. Some of the earliest comparisons between theory and measurements were published by Allaire, Kasarda, et al. [1, 3-8]. A few papers have been published on magnetic field theory applied to magnetic bearings by Rockwell, et al. [2]. More recent methods of calculating the load capacity and inductance have also been published [9, 10]. However, not many studies involving the specific design of magnetic bearings have been published on the industrial rotating machines as that information is often regarded as proprietary by the manufacturers or the magnetic bearing vendors, such as Allaire, et al [11]. This paper is intended to bring more information on industrial magnetic bearing design to the future users of magnetic bearings for high speed machinery.

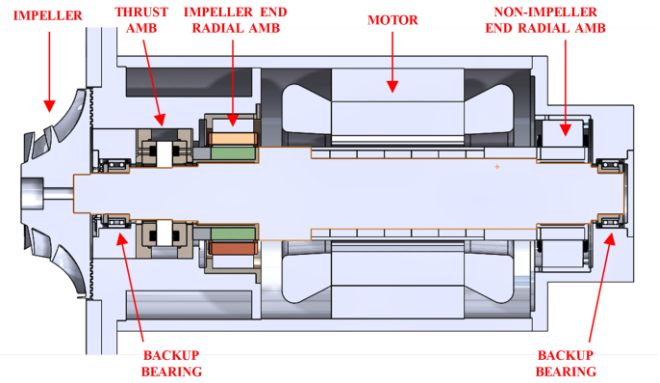

Figure 1. Schematic Design Drawing of High Speed Motor-Compressor Geometry

II. RADIAL BEARING DESIGN METHODOLOGY

A. Circuit Models

Electromagnetic AMBs operate based on Ampere's Law which relates the magnetic flux density in a closed loop circuit to the electrical current passing through the circuit. Typically, a radial AMB is designed to be operated with four quadrants, as shown in Fig. 3. Each quadrant consists of a number of poles wound in series. In isolation, the force imparted on the rotor by a single quadrant is proportional to the square of the coil current and magnetic flux density developed within that quadrant. In order to linearize the actuator's force with respect to coil current, traditionally all electromagnetic AMBs are designed as double-acting, utilizing two opposing quadrants per control axis. An equal and constant bias current is applied to all quadrants. A time-varying control current is then added to the bias current in one quadrant and subtracted from the bias current in the opposing quadrant. In this way,

the AMBs force along a given axis is linear with respect to the

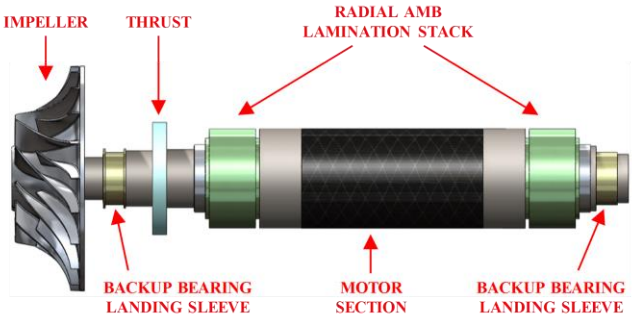

Figure 2. Motor Compressor Rotor Geometry

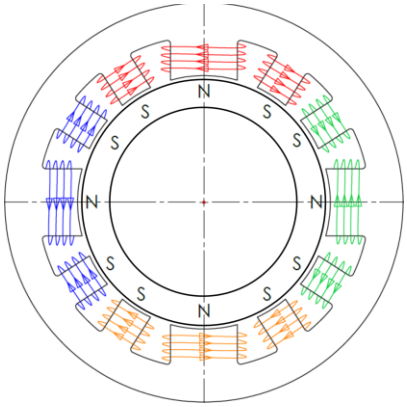

Figure 3. 12-pole, E-core design and pole configuration

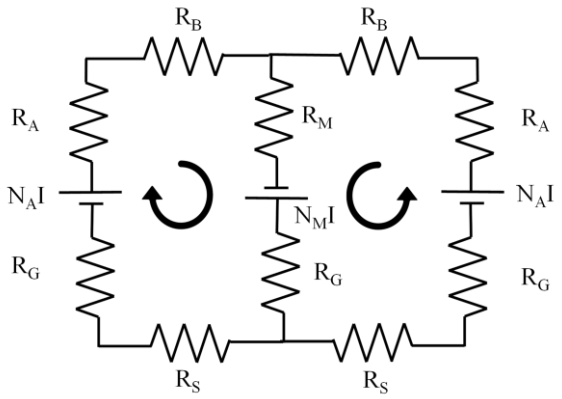

Figure 4. E-core quadrant circuit model

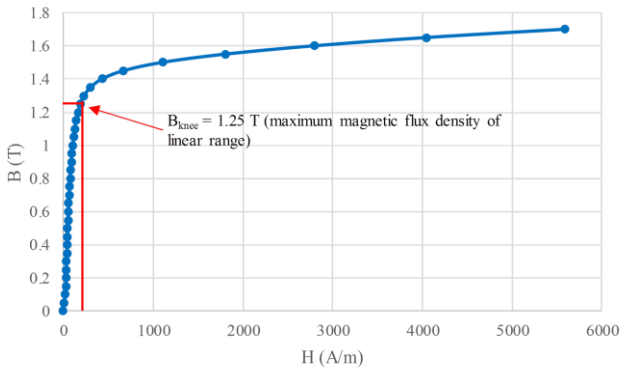

Figure 5. M19 silicon iron BH-curve illustrating linear operating range

control current. This linear operation is highly desirable from an industrial controller design stand point.

Typically, electromagnetic radial AMBs are either designed with an 8-pole, C-core pole configuration or a 12-pole, E-core pole configuration. A 12-pole, E-core configuration has been shown to have superior power density to the 8-pole design, producing similar load capacities with a smaller overall bearing size envelope. The 12-pole design was therefore chosen for this application in order to minimize actuator size. In the 12-pole design, each quadrant, or E-core, consists of a main pole flanked by two smaller auxiliary poles. These three poles are wound in series such to create an N-S-N, or S-N-S, magnetic pole arrangement. The entire actuator consists of four quadrants. Figure 3 illustrates the 12-pole E-core design and pole configuration. Here, the red and orange wound quadrants work together to control the shaft along one axis, while the blue and green wound quadrants work together to control the shaft along an orthogonal axis.

Ampere's Loop Law relating the magnetic flux density developed in a single quadrant to the current passing through the coil windings can be represented schematically by a simple 1D circuit model. Figure 4 illustrates the 1D circuit models for a single quadrant of an E-core design. The magnetomotive force developed in each pole is equal to the number of wire turns around that pole times the electrical current supplied to the windings. For each quadrant, the total MMF in each loop is equal to the total magnetic reluctance in the circuit loop. The reluctance of the soft metal components of the back iron, poles, and shaft, illustrated as R_B, R_P, and R_S, are significantly lower than the magnetic reluctance of the air gap, R_G, and can therefore justifiably be neglected. The reluctance of the air gap is related to the magnetic flux density in the gap, B_G, the length of the nominal gap, g_0, and the permeability of free space, μ_0, as given by Equation 1:

$$R_G = \frac{B_G g_0}{\mu_0} \tag{1}$$

The total MMF developed by a single quadrant of a 12-pole E-core bearing can be found by applying Ampere's Loop Law to the circuit shown in Fig. 4 and is given by Equation 2:

$$(N_M + N_A)I = \frac{2B_G g_0}{\mu_0} \tag{2}$$

Both sides of this circuit produce the same relationship given by Equation 2 due to symmetry. Again, the reluctance of the back iron, main pole, auxiliary pole, and shaft (i.e. R_B, R_M, R_A, R_S) are neglected. Here, the number of turns associated with the main pole, N_M, and the two auxiliary poles, N_A, are added together. The number of turns on the auxiliary poles compared to the main pole should be specified to generate an approximately even flux density in all air gaps and is typically between 50-60% of the main pole turns.

Typically, the magnetic flux density in the air gap is designed as the maximum linear magnetic flux density located

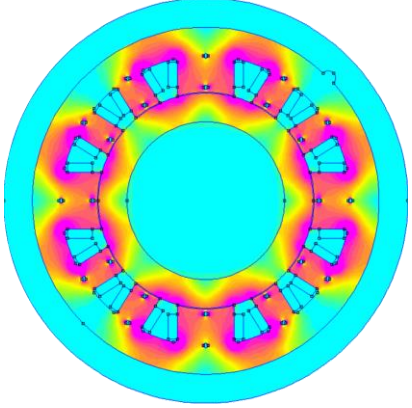

Figure 6. Calculated no-load, bias current only magnetic flux density

at the "knee" of the BH curve for the soft iron lamination material, as illustrated in Fig. 5. This magnetic flux density is achieved at the maximum operating current, *I*, for the chosen winding wire. These parameters, along with the nominal air

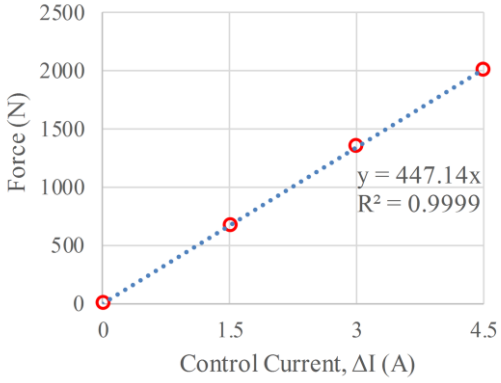

Figure 8. Radial AMBCurrent Gain

gap distance, g_0, determine the number of windings required per pole, *N*.

The physical force developed by a single quadrant is related to the square of the magnetic flux density developed in each air gap, B_G, times the area of the air gap (also pole face area), A_G, summed over all poles as given by Equation 3:

$$F_{design} = \frac{1}{2\mu_0} \sum B_i^2 A_{G_i} \qquad (3)$$

where the subscript, *i* denotes each pole. Again, using the maximum linear magnetic flux density of the soft iron material, the area of each pole's air gap can be derived from the actuator design load. It is clearly seen here that for a given soft iron lamination material, a larger design force will require a larger pole face area. For the 12-pole, E-core design, the pole face area of the auxiliary poles is designed to be approximately half of that of the main poles; therefore, the width of the auxiliary poles is typically one half the width of the main poles.

An automated bearing design method uses these derivations to generate optimal AMB geometries for a given design load, and uses 2D FEA to verify the results. The

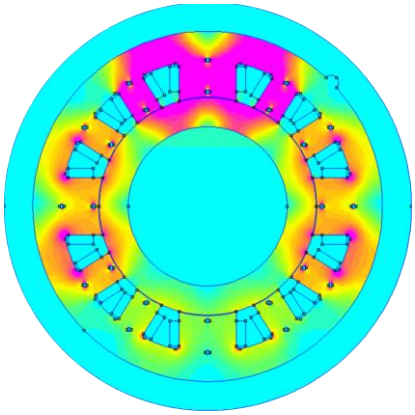

Figure 7. Calculated design load magnetic flux density (2,004 N upward)

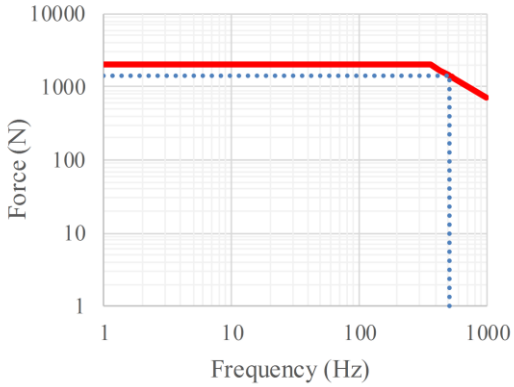

Figure 9. Radial AMB Bandwidth

required magnetomotive force and pole face area is initially calculated from the 1D magnetic circuit model based on Ampere's Loop Law. While the 1D circuit model analysis is used in the early design phase to develop initial radial bearing geometry for a given design load, it is necessary to compare the results of these simple models to the results of the 2D FEA in order to increase pole face area to meet the required design load, if necessary. A software program automates this optimized AMB design process. Based on a few simple inputs such as shaft diameter, lamination diameter or axial length, air gap length, and lamination material, the algorithm generates the proper bearing geometry, including pole winding properties, to achieve a given bearing design load. In addition to bearing geometry, the algorithm also computes AMB properties such as current gain, bandwidth, open loop stiffness, and electrical losses. The resulting radial AMB design and calculated properties are presented in the following sections. The thrust bearing is designed and presented using a similar design methodology.

B. Design and 2D FEA Analysis

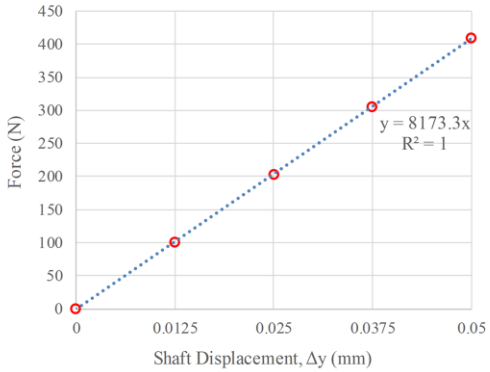

Figure 10. Radial AMB Open Loop Stiffness

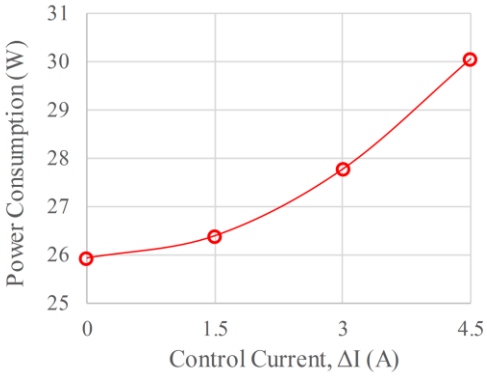

Figure 11. Coil current power losses for radial AMB

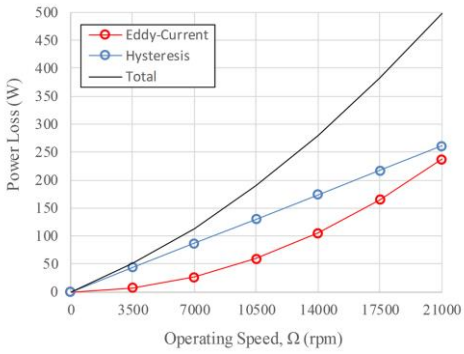

Figure 12. M19 silicon iron BH-curve illustrating linear operating range

The shaft diameter at the radial AMB locations is designed to be 98 mm. A radial AMB assembly sleeve was designed to hold both the radial lamination stack and radial sensor target ring for ease of assembly. The ID and OD of the lamination stack are used as inputs to the design algorithm and are designed to be 110 mm and 150 mm, respectively. Based on force and moment balance calculations of the rotor assembly including both the static weight of the rotor assembly and the anticipated dynamic unbalance loads, each radial AMB is designed for a load capacity of 2,000 N. The AMB is designed such that a single bearing quadrant can support the entire design load. The radial air gap between the stator poles and centered rotor is 0.5 mm. Both the rotor and stator laminations are constructed of M19 silicon-iron.

Power amplifiers were selected with a 240 VAC AC input, 160 VDC DC bus voltage, and 25 A peak current. The maximum continuous current for the amplifiers is one-half of the peak current, or 12.5 A. The radial AMBs are design to operate with a bias current of 8 A, and a control current of ±4.5 A. The AMB is designed to support the design load of 2,000 N at a control current of 4.5 A, where the maximum continuous current of 12.5 A is reached.

Table 1 presents the calculated AMB geometries and design specifications. The actuator length is calculated to be 66.5 mm while the stator back iron diameter is calculated to be 242 mm. These dimensions comprise the basic radial AMB size envelope. It should be noted that while the stator lamination stack length is taken to be the calculated 66.5 mm, a few millimeters are typically added to the rotor lamination stack to account for end leakage effects. In this case, the radial AMB rotor lamination stack is designed to be 71.5 mm. Table 1 also provides the number of winding turns for both the main and auxiliary quadrants. Figures 6, 7 illustrates the calculated magnetic flux density developed in the radial AMB during the no-load, bias current only condition, and design load condition, respectively. As seen in Fig. 6, equal bias currents in all quadrants produce an even flux density distribution and no net force of the rotor. As seen in Fig. 7, the back iron and poles of the upper quadrants near saturation at the design load. In this illustration, the simulated load is downward with the bearing magnetic force acting upward on the rotor. Small holes located in each pole for tying in the coil windings and a semicircular alignment feature along the stator OD can be seen in both figures and have a negligible effect on bearing performance.

TABLE I. CALCULATED RADIAL AMB PROPERTIES AND DESIGN SPECIFICATIONS

	Parameter	Value
D_{shaft}	Shaft Diameter*	110 mm
$D_{lamination}$	Rotor Lamination OD	150 mm
$D_{backiron}$	Stator OD	242 mm
$L_{actuator}$	Actuator Length	66.5 mm
N_{main}	Main Pole Wire Turns	36
$N_{auxiliary}$	Auxiliary Pole Wire Turns	28
$N_{quadrant}$	Total Wire Turns/Quadrant	92
ΔI_{design}	Perturbation Current	4.5 A
F_{design}	Design Force	2000 N

*Includes Shaft Sleeve

The current gain is an AMB property that is equivalent to the increase in the attractive force of the actuator along one control axis over the increase in control current supplied to the two opposing quadrants controlling motion in that axis. The current gain is not only required for designing the AMB controller, but it also proportional to the bandwidth of the AMB. Figure 8 illustrates the current gain plot for the radial AMB design. It should be noted that the current presented in Fig. 8 is the control current supplied to each of the two quadrants controlling a single axis. The bias current to all quadrants in this design is considered to be 8 A. At the design

load, a control current of 4.5 A is added to one quadrant, producing 12.5 A in that quadrant, and subtracted from the opposing quadrant, producing 3.5 A in that quadrant. A single quadrant current of 12.5 A at the design load of 2,000 N corresponds to the maximum continuous current of the selected power amplifiers. As seen as the slope of the control current to force curve in Fig. 8, the current gain is calculated as 447 N/A. The current gain is linear through the entire control current range which is necessary for a linear control scheme.

Figure 9 illustrates the bandwidth plot for the radial bearing design. The bandwidth of an AMB is defined by the actuator slew rate. As defined in Equation 4, the slew rate, or rate of change of force with respect to time, achievable by the actuator is equal to the current gain, K_i, times the current rate of change. Also shown in Eq. 4, the rate of change of current is equal to the power amplifier voltage, V, divided by the inductance of the coil windings, L.

$$\frac{dF}{dt} = K_i \frac{di}{dt} = K_i \frac{V}{L} \tag{4}$$

Based on the FEA results, the inductance of the coil windings in each quadrant is calculated to be 0.016 H. Using this value and the 160 V rated DC bus voltage of the selected power amplifiers, the radial bearings are calculated to have a half-power bandwidth of 510 Hz, as shown in Fig. 9. This bandwidth gives a 46% margin over the maximum operating speed of 21,000 rpm and should be sufficient for continuous bearing operation at peak speed. The total MMF developed by a single side can be found by applying Ampere's Loop Law to the circuit shown in Fig. 4.

The open loop stiffness, K_s, is another AMB property necessary for controller design and is equal to the change in force imparted by the actuator on the rotor over small changes in displacement of the rotor during zero-load, bias current only actuator operation. In order to calculate the open loop stiffness of the AMB, the algorithm perturbs the rotor position for a number of locations from its centered position up to 10% of the radial air gap and performs 2D FEA analysis at each position. Figure 10 illustrates the calculated displacement versus force plot for both radial bearing design, based upon the FEA results. For the radial AMB design, the open loop stiffness value is calculated as the slope of the curve to be -8,173 N/mm. Since AMBs can only produce attractive forces along their control axes, the open loop stiffness value is always taken as a negative value. As seen in Fig. 10, there is a linear relationship between force and displacement for small displacements, as shown by the linear fit.

It is important to calculate the ohmic losses that occur in the coils during operation. As control currents are increased under increasing loads, coil losses are functions of the load acting on the actuator. Figure 11 illustrates the coil losses of the radial AMB design as a function of load. The power consumption of each radial AMB ranges between 26 and 30 W depending on the external load. This power consumption is considered quite low. In addition to operational power losses in the AMB coils, electrical losses in the laminations of the rotor and stator occur due to hysteresis effects and eddy-current losses. These losses are carried by the driving motor of the shaft. It is important to quantify these losses to appropriately size the machine motor. As illustrated in Figure 12, these hysteresis and eddy-current losses are functions of rotational speed with both losses increasing with increasing speed. The total electrical losses of each radial AMB reach a maximum of 500 W at the maximum rotational speed of 21,000 rpm. These relatively small losses represent only a fraction of 1 percent of the 200 KW motor unit.

III. Thrust Bearing Design Methodology

A. Circuit Models

Typically, all electromagnetic thrust AMBs are designed in C-core configurations following a similar design methodology as previously presented for the radial AMB design. Figure 13 presents a simple schematic including magnetic flux paths of the C-core thrust bearing design. Back iron components on either side of the thrust disk wrap circumferentially around the shaft and contain their own coil windings. The coil windings on either side of the disk are wound in opposing directions. In reference to Fig. 13 this winding arrangement produces a S-pole on the lower side of the back irons closest to the shaft and a N-pole on the upper side of the back irons. The two C-core back irons work together to control axially motion of the shaft using bias and control currents similar to those previously discussed for the radial bearing.

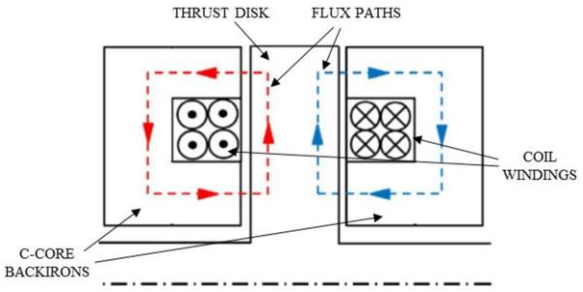

Figure 13. Thrust bearing pole and coil winding

Again, Ampere's Loop Law relating the magnetic flux density developed in a single C-core back iron side to the current passing through the coil winding can be represented schematically by a simple 1D circuit model. Figure 8 illustrates the 1D circuit models for a single sided C-core design. Like the radial bearing, the magnetomotive force developed in each pole is equal to the number of wire turns in each side of the thrust stator times the electrical current supplied to the windings. For each side, the total MMF in each loop is equal to the total magnetic reluctance in the circuit loop where the reluctance of all soft metal components is justifiably ignored. For the C-core thrust AMB design, the total MMF developed by a single side can be found by applying Ampere's Loop Law to the circuit shown in Fig. 14 and is given by Equation 5:

$$NI = \frac{B_G g_0}{\mu_0} \tag{5}$$

The optimized design method based upon these equations was used to generate the optimal thrust AMB geometries using 2D FEA to verify the results. Based on a few simple inputs such as shaft diameter, air gap length, and lamination

material, the algorithm generates the proper bearing geometry, including winding properties, to achieve a given bearing design load. In addition to bearing geometry, the algorithm also computes AMB properties such as current gain, bandwidth, open loop stiffness, and operational power losses. The resulting thrust AMB design and calculated properties are presented in the following sections.

B. Design and 2D FEA Analysis

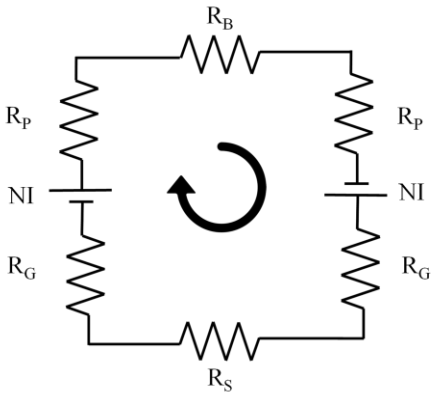

Figure 14. Magnetic circuit diagram for thrust bearing

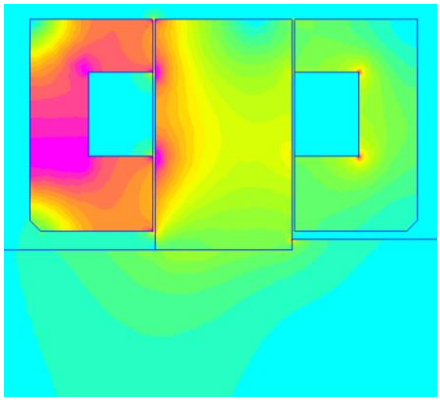

Figure 16. Thrust bearing magnetic flux plot at design load of 3,000 N

The shaft diameter at the thrust AMB location is designed to be 84 mm. Based on estimated axial load calculations provided by Palboom, the thrust AMB is designed for a load capacity of 3,000 N. The radial air gap between the stator poles and centered rotor is 0.5 mm. The stator back iron components are constructed of M19 silicon-iron. The thrust disk is considered to be AISI 4340 steel with oil quenched heat treatment for increased strength to handle high stress loads.

The same power amplifiers used for the radial AMBs will be used for the thrust AMB. Again, these power amplifiers have a 240 VAC AC input, 160 VDC bus voltage, and 25 A peak current. Like the radial AMBs, the thrust AMB is designed to operate with a bias current of 8 A, and a control current of ±4.5 A. The AMB is designed to support the design load of 3,000 N at a control current of 4.5 A, where the maximum continuous current of 12.5 A is reached. Like the radial AMBs, very brief instances of force overloads can be handled by pushing the control current to ±8 A. An absolute maximum current of 16 A would work to overheat the amplifiers and is not sustainable for any substantial period of time. This short period, overload capacity is discussed later in this paper.

Table 2 presents the calculated AMB geometries and design specifications. The overall actuator length is calculated to be 72.4 mm while the actuator outer diameter is calculated to be 170 mm. These dimensions comprise the basic thrust

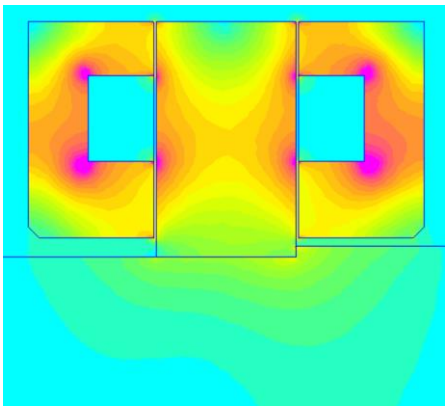

Figure 15. Thrust bearing magnetic flux plot with equal coil currents

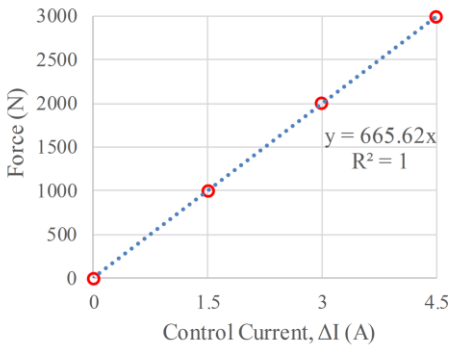

Figure 17. Current gain for thrust bearing

AMB size envelope. Table 2 also provides the number of winding turns per stator side as 63 turns.

TABLE II. CALCULATED THRUST AMB PROPERTIES AND DESIGN SPECIFICATIONS

	Parameter	Value
D_{shaft}	Shaft Diameter	84 mm
$ID_{back\ iron}$	Back Iron ID	91 mm
$L_{backiron}$	Back Iron Axial Length	22.9 mm
L_{disk}	Thrust Disk Axial Length	25.6 mm
$OD_{actuator}$	Actuator OD	170 mm
N_{side}	Turns Per Thrust Side	63
ΔI_{design}	Perturbation Current	4.5 A
F_{design}	Design Force	3000 N

Figures 15 and 16 illustrate the calculated magnetic flux density developed in the thrust AMB during the no-load, bias current only condition, and design load condition,

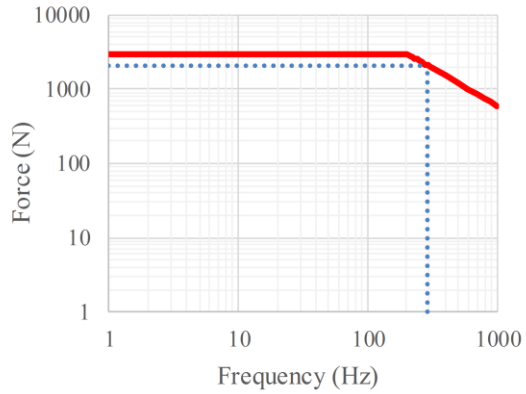

Figure 18. Thrust bearing bandwidth

respectively. As seen in Fig. 15 equal bias currents to both sides produce an even flux density distribution and thus no net force of the rotor. As seen in Fig. 16, the left side back iron poles near saturation at the design load. In this illustration, the simulated load is rightward acting with the bearing magnetic force acting leftward on the rotor.

Figure 17 illustrates the current gain plot for the thrust AMB design. It should be noted that the current presented in Fig. 13 is the control current supplied to each of the two sides of the thrust bearing. The bias current to both sides in this design is considered to be 8 A. At the design load, a control current of 4.5 A is added to one side, producing 12.5 A in that side, and subtracted from the opposing side, producing 3.5 A in that side. A single side current of 12.5 A at the design load of 3,000 N corresponds to the maximum continuous current of the selected power amplifiers. As seen as the slope of the control current to force curve in Fig. 17, the current gain is calculated as 665 N/A. The current gain is linear through the entire control current range which is necessary for a linear control scheme.

Figure 18 illustrates the bandwidth plot for the thrust bearing design. Based on the FEA results, the inductance of

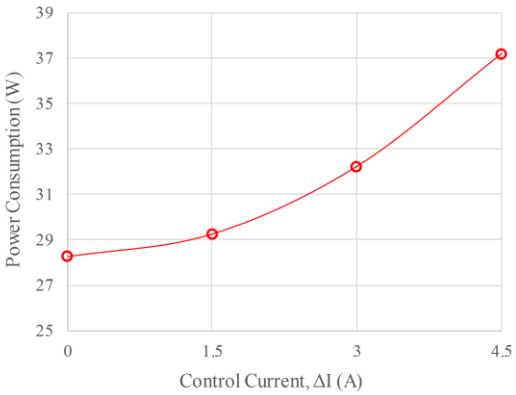

Figure 20. Operational Power Loss of Thrust Bearing

the coil windings on each side of the thrust bearing is calculated to be 0.028 H. Using this value and the 160 V rated DC bus voltage of the selected power amplifiers, the radial bearings are calculated to have a half-power bandwidth of 286 Hz, as shown in Fig. 18. This value gives an approximately 0.8x bandwidth in relationship to the maximum operating speed of 21,000 rpm. Typical dynamic thrust loads occur at very low frequencies far below the maximum 1x frequency of 350 Hz in this machine. The 0.8x bandwidth should be sufficient for continuous bearing operation at peak speed.

Figure 19 illustrates the calculated displacement versus force plot for the thrust bearing design, based upon the FEA results. For the thrust AMB design, the open loop stiffness value is calculated as the slope of the curve to be -9,552 N/mm. As seen in Fig. 19, there is a linear relationship between force and displacement for small displacements, as shown by the linear fit.

Figure 20 illustrates the operational coil power losses of the thrust AMB design as a function of load. The power consumption of the thrust AMB ranges between 28 and 37 W depending on the external load. This power consumption is considered quite low and is easily handled by the powering amplifiers.

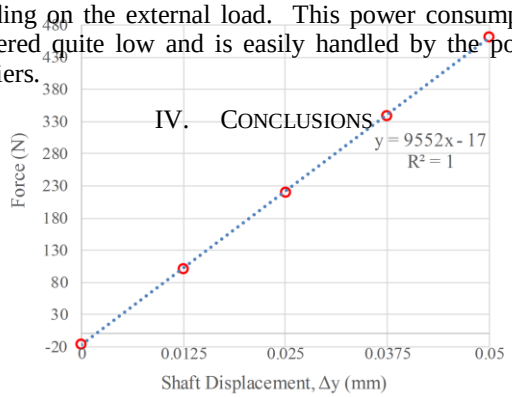

Figure 19. Thrust bearing Open Loop Stiffness

IV. Conclusions

This paper presents the magnetic bearing design properties of a high speed motor compressor magnetic bearing design. Significant detail is presented to illustrate how the basic magnetic bearing design properties are evaluated to meet the desired load capacity of the bearings while optimizing the bearing in terms of minimum magnetic bearing size, given the rotor diameters and other parameters

References

[1] P. E. Allaire, R. L. Fittro, E. H. Maslen, and W. C. Wakefield, "Measured Force/Current Relations in Solid Magnetic Thrust Bearings," *Journal of Engineering for Gas Turbines and Power*, vol. 119, no. 1, pp.137-142, 1987.

[2] R. D. Rockwell, P. E. Allaire, J. C. Heinrich, and G. K. Foshage., "Magnetic Field Modeling of Magnetic Bearings Including Rotor

Motion Effects and Eddy Currents," *Proceedings of the Fifth International Symposium on Magnetic Bearings*, pp. 241-246, 1996

[3] P. E. Allaire, M. E. F. Kasarda, E. H. Maslen, and G. R. Gillies, "Rotor Power Loss Measurements for Hetropolar and Homopolar Magnetic Bearings," *Proceedings of the Fifth International Symposium on Magnetic Bearings*, pp. 271-276, 1996

[4] R. L. Fittro, D. O. Baun, E. H. Maslen, and P. E. Allaire, "Calibration of an 8-Pole Planar Radial Magnetic Actuator," *Proceedings of ASME International Gas Turbine and Aeroengine Congress and Exhibition*, 1997

[5] P. E. Allaire, M. E. F. Kasarda, E. H. Maslen, G. R. Gillies, and L. K. Fujita, "Flux Density and Air Gap Effects on Rotor Power Loss Measurements in Planar Radial Magnetic Bearings," *Proceedings of ASME International Gas Turbine and Aeroengine Congress and Exhibition*, 1997.

[6] P. E. Allaire, M. E. F. Kasarda, and L. Fujita, "Rotor Power Losses in Planar Radial Magnetic Bearings - Effects of Number of Stator Poles, Air Gap Thickness, and Magnetic Flux Density," *Proceedings of ASME International Gas Turbine and Aeroengine Congress and Exhibition*, 1998.

[7] P. E. Allaire, M. E. F. Kasarda, and L. Fujita, "Rotor Power Losses in Planar Radial Magnetic Bearings - Effects of Number of Stator Poles, Air Gap Thickness, and Magnetic Flux Density," *Journal of Engineering for Gas Turbines and Power*, vol. 121, no. 4, pp. 691-696, 1999.

[8] M. E. F. Kasarda, P. E. Allaire, P. M. Norris, C. Mastrangelo, and E. H. Maslen, "Experimentally Determined Rotor Power Losses in Homopolar and Heteropolar Magnetic Bearings," *Journal of Engineering for Gas Turbines and Power*, vol. 121, no. 4, pp. 697-701, 1999

[9] T. W. Dimond, R. Rockwell, G. Simmons, and P. Allaire, "Comparison of Load Capacity and Inductance for Common Active Magnetic Bearing Designs," *Proceedings of the Twelth International Symposium on Magnetic Bearings*, 2010.

[10] T. Dimond, T. Meriwether, J. Kaplan, R. Rockwell, and P. Allaire, "Automated Design Optimization of E-core Active Magnetic Bearings," *Proceedings of the 8th IFToMM International Conference on Rotordynamics*, 2010

[11] P. Allaire, B. Nichols, T. Dimond, S. Dousti, R. Newark, N. Lloyd, O. Ashahrani, F. Daneshvar, "Design of Active Magnetic Radial and Thrust Bearings for High Speed Turbo Aerator," *Proceedings of the Fifteenth International Society of Magnetic Bearings*, 2016.